WING LEADING EDGE CONCEPTS FOR NOISE REDUCTION

Arvin Shmilovich, Yoram Yadlin, David M. Pitera
The Boeing Company

Keywords: *aerodynamics, noise, high-lift, leading-edge, slat*

Abstract

This study focuses on the development of wing leading edge concepts for noise reduction during high-lift operations, without compromising landing stall speeds, stall characteristics or cruise performance. High-lift geometries, which can be obtained by conventional mechanical systems or morphing structures have been considered. A systematic aerodynamic analysis procedure was used to arrive at several promising configurations. The aerodynamic design of new wing leading edge shapes is obtained from a robust Computational Fluid Dynamics procedure. Acoustic benefits are qualitatively established through the evaluation of the computed flow fields.

1 Introduction

Ever tightening environmental constraints and strict noise regulations have led over the years to air traffic inefficiencies and reduced airport productivity. At many airports current capacity is largely controlled by the hours of operations, which due to noise pollution are confined mostly to daylight hours. Consequently, noise reduction in airport environments has become an area of high priority in the aerospace transport industry. During takeoff, approach and landing noise is generated by the engines and various airframe components. A significant reduction in engine noise has been achieved in recent years with the advent of high bypass ratio engines. Consequently, other noise sources have become more critical, with greater focus now being placed on airframe noise reduction techniques.

A major component of airframe noise is the high-lift system, which contributes significantly to the total noise during approach and landing when the engines operate at low power setting. In particular, slotted leading edge slats produce high noise levels at these conditions. This study is aimed at the development of leading edge (LE) devices with improved noise characteristics. More specifically, it targets candidate concepts for reducing or eliminating noise of conventional slats without compromising landing stall characteristics or cruise performance. This study was performed under the NASA Multi-Objective Leading Edge Concepts (MOLEC) program and this paper will describe the development of high-lift devices with emphasis on aerodynamic aspects of the design.

System implementation is a critical element in the design of practical high-lift systems. Both short term options using state of the art mechanical systems and long term solutions based on morphing structures have been considered in the context of this investigation. The latter will require significant advances in adaptive structures in conjunction with skin technology. A wide range of leading edge concepts was first identified as possible solutions. A subsequent initial assessment with respect to aerodynamic performance, potential acoustics benefits, and viability of system mechanization has rendered a smaller set of candidate concepts worthy of further consideration. These concepts are grouped in several families of wing leading edges and they are the focus of the current evaluation. Based on the experiments conducted by Andreou, Graham and Shin [1], these types of LE devices have

demonstrated relatively low noise signatures in the wind tunnel. In this study only the aerodynamic element of the design is considered. Two-dimensional Computational Fluid Dynamics (CFD) simulations were used to develop the new cross sectional LE geometries. Validation with experimental data obtained for the baseline configuration demonstrates very good agreement in terms of forces and pressure distributions, indicating that the computational tool is adequate for high-lift design over the range of angles of attack, including maximum lift. Qualitative noise assessments are presented in the form of inferential arguments through the examination of the computed flow fields.

The paper will describe the numerical procedure and guidelines for modeling in the context of high-lift and Active Flow Control (AFC). Results of validation with experimental data will be shown for the baseline high-lift system. Three families of low-noise wing leading edge geometries will be presented, followed by description of the design methodology used to develop a set of promising candidates. A set of diagnostics tools will be employed in order to assess aeroacoustics benefits.

2 Numerical Procedure

The numerical tool is a modified OVERFLOW code originally developed by NASA [2] and it forms the core process of Boeing's transport aircraft CFD methodology. OVERFLOW employs the Reynolds Averaged Navier-Stokes (RANS) formulation using overset grid systems. Special modules have been developed by Boeing [3] for applying time-varying boundary conditions to simulate excitation due to flow control devices. Actuator flows can be described by stagnation properties and general jet velocity signals. The algorithm uses the characteristics approach for consistent application of actuator flow conditions. The numerical tool has been validated extensively for numerous high-lift applications. Flow control modeling has also been validated using a set of experiments for a range of actuation modes [3, 4].

3 Baseline Wing Section

The Energy Efficient Transport (EET) wing section developed by Lin and Dominik [5] was selected as the baseline configuration representing a conventional multi-element wing. The high-lift system shown in Figure 1 consists of slat, wing and flap elements. The EET section was optimized experimentally for maximum lift and extensively tested in the Low Turbulence Pressure Tunnel (LTPT). This high Reynolds Number wind tunnel was designed to produce high fidelity flows at close to full-scale conditions. Special side wall treatment of viscous layers ensures high-lift flows which are nearly free of tunnel wall effects.

Fig. 1. EET Wing Section

4 Validation

Two-dimensional simulations are used in both the validation step and in the subsequent design phase. A second order upwind differencing scheme and the Spalart-Allmaras turbulence model have been employed for most simulations. Fully turbulent flows are considered. The grid system for the EET airfoil is presented in Figure 2. It consists of eight overset blocks with approximately 325,000 points. C-type meshes around the respective leading edges of individual elements are used. Cap grid systems of C-type are also used around the blunt trailing edges of the flap and main wing element to ensure numerical stability for high Reynolds Number flows at maximum lift. The grid spacing perpendicular to the surface produces a $y+ \sim 1$ for the Reynolds Number considered here. Very fine mesh resolution is used in order to accurately represent the flow in the slat cove region for facilitating future acoustic analyses.

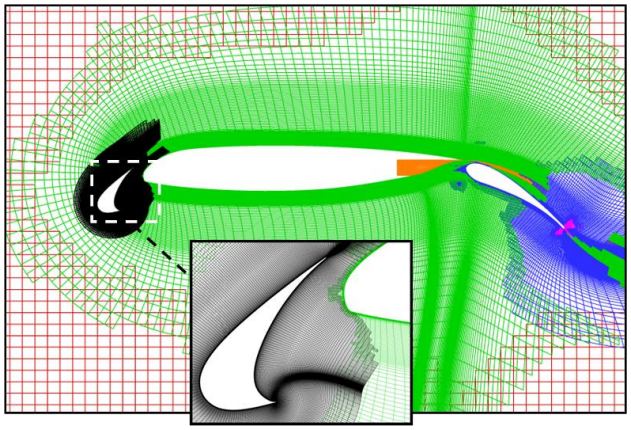

Fig. 2. Grid System for the EET Section

Free air calculations were performed for a range of angles-of-attack for a free stream Mach number of 0.2 and Reynolds Number, R_N, of 9 million based on cruise airfoil chord length. The experimental data from Reference [5] is used for validation. Figure 3 presents the lift curve and the pressure distribution at the nominal landing condition which corresponds to α=6°. Pressure distributions are well predicted, although differences with experimental data exist on the lower side of the slat. The lift curves of experimental data and simulations are in very good agreement in the linear range. Notable discrepancies exist near maximum lift

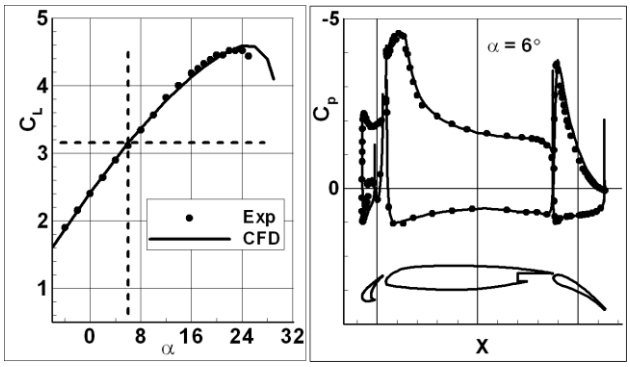

Fig. 3. Validation at the Nominal Landing Condition

conditions; there is a difference of about 1.5% in $C_{L\ Max}$, with a larger discrepancy of 8.3% in terms of $\Delta C_{L\ Max}$. Nevertheless, this agreement indicates that the numerical predictions are acceptable in the context of this study and the CFD tool is adequate for high-lift design at the nominal landing condition and at maximum lift. This is a particularly valid assumption when used on a comparative basis in order to establish relative merits.

Flow progression with increased airfoil incidence illustrating high-lift characteristics of the EET airfoil is described by total pressure flow fields in Figure 4. At the nominal landing condition the flow is well behaved over the three elements. However, flow recirculation occurs in the slat cove region, which is considered a major source of noise. At maximum lift (α=24°) the flow is still fully attached, but larger losses are evident at the main element and the flap, where stronger interactions between the various viscous layers takes place. Interestingly, flow separation at the slat has been eliminated due to the higher global circulation at this lift level whereby the stagnation point on the main element has moved downstream. From an aerodynamic stand point turning of the flow at the flap is degraded due to adverse pressure gradients the slat and main element wakes experience as they pass through the suction peak on the flap. Flow quality further deteriorates at start of stall (α=26°) where de-cambering of the streamlines leads to off surface separation at the flap, resulting in reduced lift.

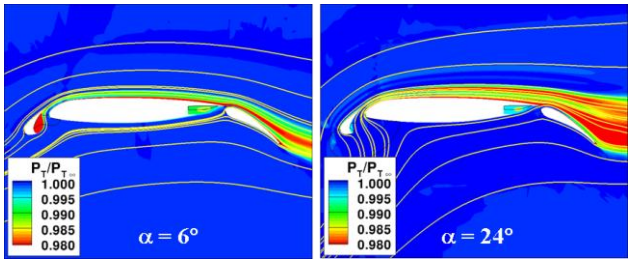

Fig. 4. Flow Characteristics of EET Section

From an operational standpoint, stall speed is a determinant of landing field length. Generally, a slower approach speed will result in a shorter field length, and the landing approach speed can be no slower than 1.23 times the 1G stall speed. This determines the lift coefficient corresponding to landing approach, also referred to as nominal landing condition. $C_{L\ Max}$ is the lift coefficient at the 1G stall speed, which is measured during flight test. Therefore modified leading edges with reduced noise at

landing approach must be evaluated at $C_{L\ Max}$ to ensure that there is no change to the stall speed.

In the current analytical study with the EET section, the lift coefficient during landing approach is 3.15 based on the estimated $C_{L\ Max}$. This lift coefficient corresponds to $\alpha=6°$, which is indicated by the dashed lines in the lift curves throughout this paper.

5 Evaluation of Potential Wing LE Configurations

The best method for developing a high-lift system is by employing a Multi-Disciplinary Optimization approach, which encompasses acoustics, aerodynamics, structures and mechanics. In this initial phase of the evaluation, however, only the aerodynamics aspects of the design are considered. Therefore, knowledge based engineering was employed throughout the aerodynamic development of candidate LE concepts in the form of inferential arguments with respect to acoustics through the examination of computed flow fields.

5.1 Design Ground Rules

The goal of this study is to develop viable wing LE concepts for reducing the noise associated with conventional leading-edge slat structures without compromising the stall characteristics at landing. A systematic approach based on wing section analysis was employed for developing most viable configuration within each family of candidates. Reduced noise is required for the condition corresponding to nominal landing operation, with lift equal or greater than that of the baseline section. Additionally, $C_{L\ Max}$ should be no lower than the baseline value.

Several ground rules have been adopted for the development of candidate configurations. The high-lift EET section is used to represent the baseline geometry in the landing configuration. The flap deflection was fixed and identical to the EET airfoil. The cruise mold lines have been preserved in order to limit the scope of the analysis to high-lift conditions. The designs are limited to LE modifications, although if needed, AFC could be placed on any wing element. No optimization of slat or flap in terms of gap or overhang was performed since the study focuses on identifying gross effects. Therefore the aerodynamic performance of final candidates should be considered conservative. The two dimensional numerical analyses use similar grids for the baseline and the new geometries in order to ensure minimal differences in discretization errors.

5.2 Design Candidates

The concepts chosen for the aerodynamic evaluation are generally grouped into three families (denoted by Series numerals) as described in Figure 5. Representative geometries are overlaid on the baseline wing section, which consists of a slotted slat.

The first candidate is the clean wing section, denoted Series 1. The second family (Series 3) consists of drooped leading edges with an upper surface definition designed to reduce propensity of flow separation. Variations of these shapes include forward extensions for added lift. These devices will require special actuators and skin technologies to facilitate the detent of the drooped LE sections. The third group (Series 2) consists of slat cove fillers designed to eliminate the shedding of the wake off the slat and maintain good flow quality in the gap. This has implications for both acoustics and aerodynamic performance. Cove fillers will also require morphing structures since they are not easily retractable due to the limited space between slat and main wing element.

Fig. 5. Candidate Geometries for Low Noise Devices

A note on noise with respect to prospective wing leading edges is in order. Generally, flow recirculation which often occurs in the slat cove region and the channel flow between the slat

and the main wing element are major sources of slat noise. Therefore, non-slotted devices like the clean section and the droop leading edges are advantageous from an acoustics perspective. Slat cove fillers are also attractive in terms of reduced acoustic signature.

5.2.1 Clean Airfoil (Series 1)

The clean airfoil represents the simplest high-lift system with no geometrical change in the LE with respect to the cruise configuration. Not surprisingly, the computed results in Figure 6 indicate that the high-lift performance is very poor, with $C_{L\ Max}$ lower than the lift of the baseline airfoil at the nominal flow condition. At high-lift conditions the flow can not effectively turn around the leading edge. The sharp pressure peak and the adverse pressure gradient impact the development of the viscous layer on the upper surface. This severely limits lift development at relatively small angles-of-attack.

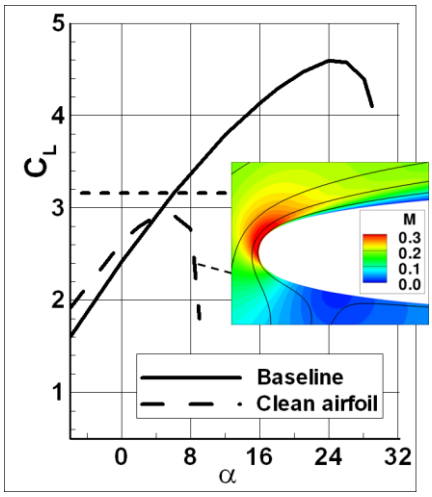

Fig. 6. Clean Section

Several studies demonstrate that passive flow control for clean single-element airfoils can enhance $C_{L\ Max}$ by delaying onset of leading edge separation. For example, passive control can be accomplished with lower-to-upper surface ducting in the leading edge region where the pressure differential drives a stream of air. According to Reference [6] this helps energize the viscous layer and postpones stall by approximately 0.2. In a similar study targeting rotorcraft applications a $\Delta C_{L\ Max} \approx 0.4$ was experimentally obtained [7]. While these gains might be suitable for certain applications, they are quite modest and we consider them totally inadequate for airplane applications.

5.2.2 Droop Leading Edge (Series 3)

Several variants of droop leading edges have been considered. Geometries and accompanying lift curves are presented in Figure 7. Airfoil modifications were confined only to the region upstream of the 0.133 chord station, which corresponds to the slat trailing edge in the stowed position. Configuration 3a represents a droop LE of 30° with a small extension of 1.6% airfoil chord. This definition is similar to the airfoil investigated in References [4] and [8]. Configuration 3c is a droop LE defined by the outer surface of the baseline slotted slat. It consists of a 25.8° droop and a 10% chord extension. Airfoil 3c-mod2 represents a large chord extension of 17.3% chord with a droop of 35°. To help reduce propensity of flow separation at large incidence, upper surface definitions between slat and main element use small surface curvature in the 3c and 3c-mod2 definitions.

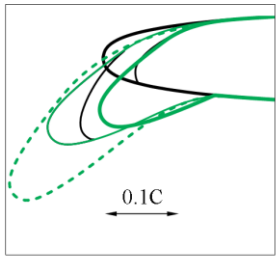

	Droop	Extension (x/c)	$C_{L\ Max}$
3a	30°	1.6	3.7
3c	26°	10.0	3.8
3c-mod2	35°	17.3	4.2

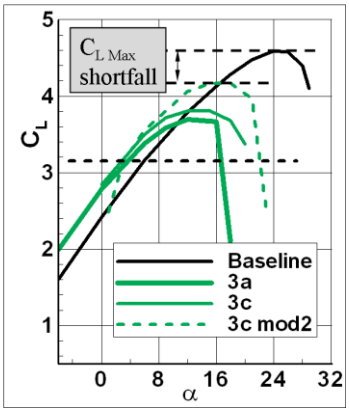

Fig. 7. Drooped Slats (Series 3)

At relatively low angles-of-attack the drooped slats are more effective in producing higher lift at constant incidence. On the other hand, the slotted slat of the baseline airfoil is very efficient in terms of maintaining attached flow up to very high angles-of-attack. Maximum lift is relatively low for all drooped slats. However, the combination of large

extension and large droop angle of 3c-mod2 helps achieve a maximum lift of 4.16, which is about 0.45 lower than that of the baseline airfoil.

Figure 8 shows the pressure distributions at α=15°. The 3c-mod2 slat produces low suction levels at the LE and in the hinge region, resulting in a healthier boundary layer on the upper surface and higher maximum lift relative to the other droop slats. At low angles-of-attack, though, the flow on the lower surface of 3c-mod2 tends to separate due to the small LE radius. However, we believe this can be relatively easily fixed by re-contouring of the surface in order to produce larger LE radius.

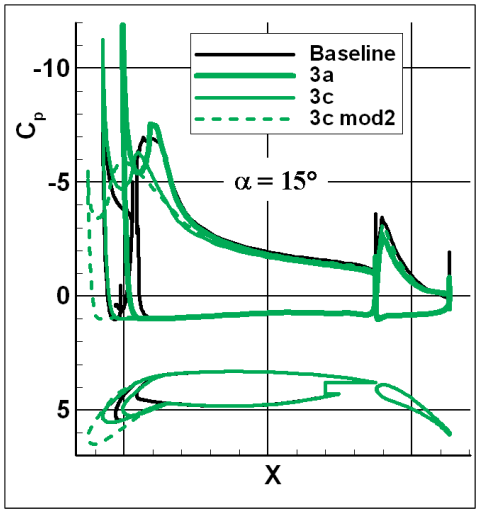

Fig. 8. Pressure Distributions for Drooped Slats

As mentioned earlier, drooped LE slats are attractive because of their reduced acoustic signature. It is therefore desirable to enhance performance of promising droop slats in order to achieve maximum lift level comparable to that of the baseline airfoil. Boeing has previously used AFC to demonstrated improved high-lift performance for multi-element airfoils [4, 8, 9]. This option was evaluated in the current study in conjunction with 3c-mod2.

Two port layouts were considered. In one application an upper surface port in the hinge region between slat and main wing element was used. In a second implementation an array of three equally spaced ports were placed on the upper surface of the flap. Various actuation modes were provided in the form of constant suction, constant blowing and pulse zero mass flow (ZMF). Although the objective wasn't to optimize AFC modes for best aerodynamic performance, a couple of actuation parameters were used to assess sensitivities to jet intensities and frequency of actuation in the ZMF case. Pulsed actuation didn't produce significant variations in $C_{L\,Max}$ with frequency of actuation.

The most effective mode of actuation was obtained with constant blowing using flap actuation. Figure 9a shows lift curves obtained with combinations of ports using constant blowing. The numerical simulations were performed according to the procedure described in References [3] and [9]. Ports are embedded into the flap with orifices oriented at ~23° relative to the local flap surface. A momentum coefficient of C_μ=0.014 is used at each port. Actuations applied at the front port, the two forward ports and the three ports are shown. As expected, aerodynamic performance increases with number of ports employed, indicating that the two-port actuation is adequate for attaining the target $C_{L\,Max}$. It should be noted that the nominal landing condition requires a lift of 3.15 in order to maintain required lift margin to $C_{L\,Max}$ of 4.6. In other words, the angle-of-attack for the nominal condition of airfoil 3b-mod2 with two AFC ports is ~1.5°.

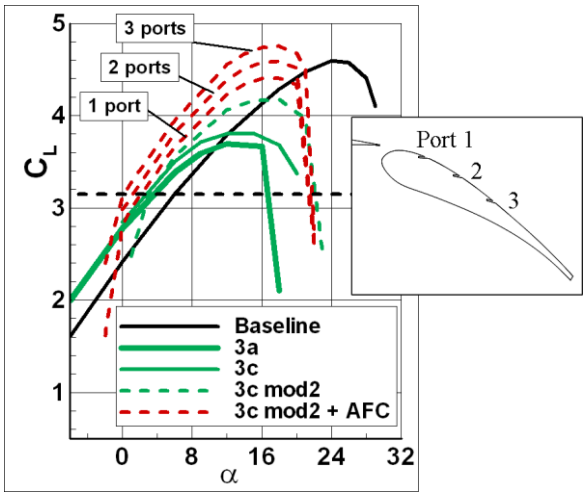

Fig. 9a. Lift Curves for Droop Slat 3c-mod2 with AFC

Figure 9b presents the Mach number contours for the uncontrolled 3c-mod2 case and the 3-port flow controlled case at the α=16° condition which corresponds to maximum lift. The momentum engendered into the flow due to actuation helps energize the viscous layers and more efficient flow turning is obtained in the aft region. This results in increased global circulation and higher lift.

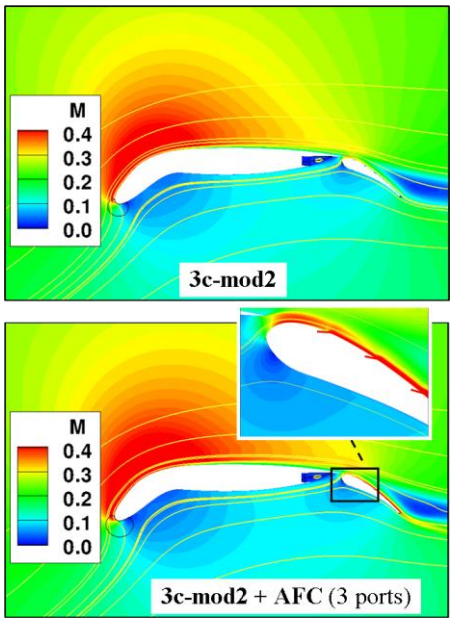

Fig.9b. Effects of AFC for Drooped Slat 3c-mod2

5.2.3 Slat Cove Fillers (Series 2)

Slat cove fillers for reduced noise have been investigated at several research institutes and academic outfits. When correctly applied, slat cove filler averts flow recirculation and thus eliminates one of the noise generation sources. Generally, experiments demonstrate that meaningful reduction in noise levels can be obtained, depending on filler types and implementation. Important contributions were made recently by NASA and Boeing [10], EADS [11] and JAXA [12].

5.2.3a α-Fillers

In this study a two-step systematic approach is adopted in order to define a family of cove fillers. This process is illustrated in Figure 10. It starts with the flow solution obtained for the baseline airfoil at a given α (hence dubbed α-filler). In the first step the boundary of the

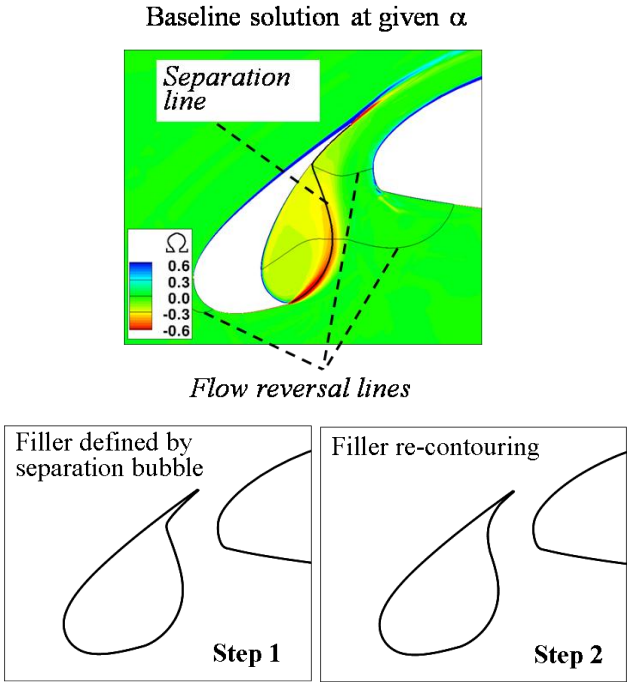

Fig. 10. Process for Definition of Slat Cove Fillers

separation pocket in the slat cove is then used to define the shape of the initial filler. The solution obtained for this slat filler is analyzed and a refined version of the filler is subsequently used in the second step, followed by a final flow analysis. The latter step is crucial for improving flow quality in the channel between slat and main element and it has implications for both acoustics and aerodynamic performance.

Step 1

In the first step, four slat fillers were defined from the baseline solutions obtained for the 0º, 6º, 12º and 18º angles-of-attack. Cove filler definitions are obtained from the respective flow separation lines. The fillers are designated by the respective angle-of-attack, i.e., the filler obtained from the α=6º is denoted 2bα06. Point analyses are presented in Figure 11 where the flow fields and the aerodynamic characteristics are obtained for the particular values of angle-of-attack. The flow fields of each the slat fillers are compared with the respective baseline case in Figure 11a. The flow fields are described by vorticity contours, regions of flow reversal (negative streamwise velocity component) and select streamlines. In each of the α cases,

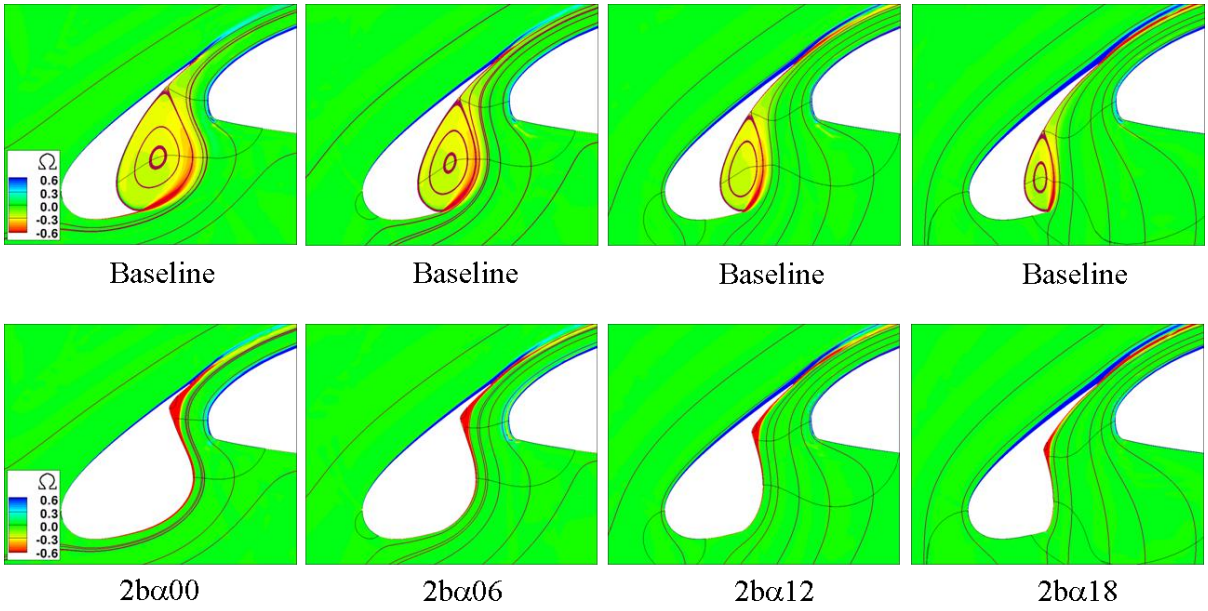

Fig. 11a. Flow Field of Baseline Airfoil and Slat Fillers at the Corresponding Angles of Attack (Step 1)

solutions indicate that the flow structure outside of the separation pocket of the baseline airfoil is very similar to its filler counterpart. The advantage of slat fillers is that flow separation and the wake off the lower side of the slat are removed, with commensurate implications to acoustics characteristics.

Consistent with the flow fields in Figure 11a, the lift levels in Figure 11b indicate that the slat fillers produce global flow characteristics also similar to the baseline airfoil. Interestingly, the fillers result in lower drag levels. This is especially noticeable in the smaller α cases, in which the strong wakes emanating from the lower trailing edge of the original slat are outright eliminated by the fillers.

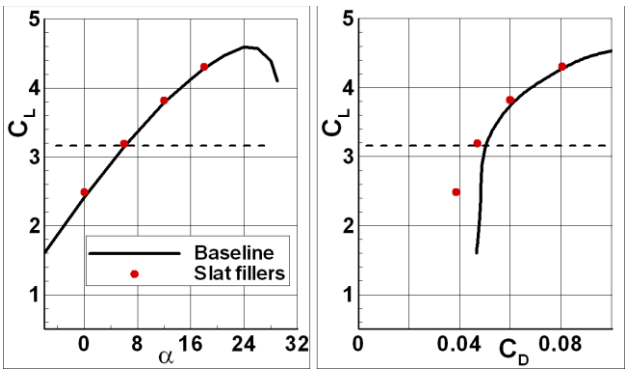

Fig. 11b. Aerodynamic Forces of Baseline Section and Slat Cove Fillers (Step 1)

Next, the aerodynamic performance of each of the slat fillers is evaluated over the range of angles-of-attack. Figure 12a shows the flow fields at the nominal condition (α=6º) and at maximum lift (α=24º). Figure 12b presents the lift curves and the drag polars. All slat fillers produce lift similar to the original airfoil at the nominal landing condition. However, the smallest filler 2bα18 is not acceptable since it results in shedding of a wake from the lower side of the slat, potentially a noise generation source and defeating the purpose of this exercise. In terms of stall characteristics, the larger the filler the lower the maximum lift. Clearly, filler 2bα00 shows the largest penalty, whereas 2bα12 results in less than 0.1 reduction in $C_{L\,Max}$ relative to the baseline.

Parametric summary of the cove fillers is presented in Figure 13 in terms of intensity of the wake emanating from the slat edge at α=6°. Wake intensity is used here as proxy of potential noise generation mechanism with the understanding that a complete acoustics evaluation can only be obtained via aeroacoustics analysis or testing. Nevertheless, at this stage wake intensity will be used as a guide for further refinements of the fillers. The wake intensity in Figure 13 is represented by maximum vorticity magnitude and by vorticity differential across the wake at the 0.017c station

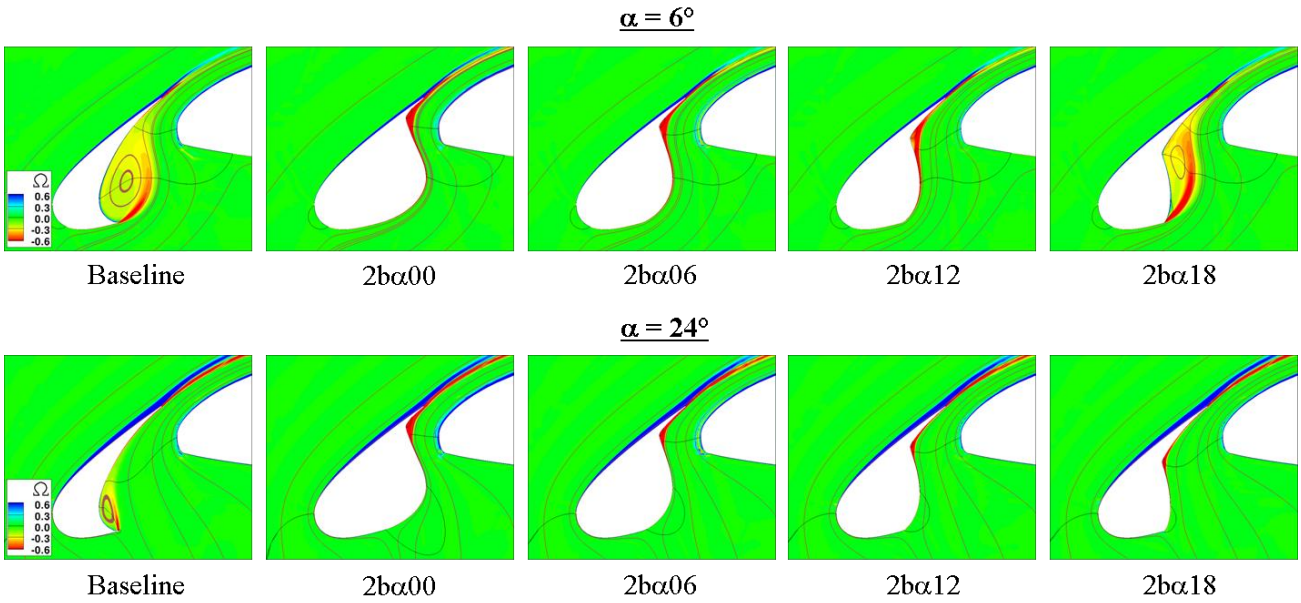

Fig. 12a. Flow Fields of Slat Fillers at the Nominal Condition and Near $C_{L\ Max}$ (Step 1)

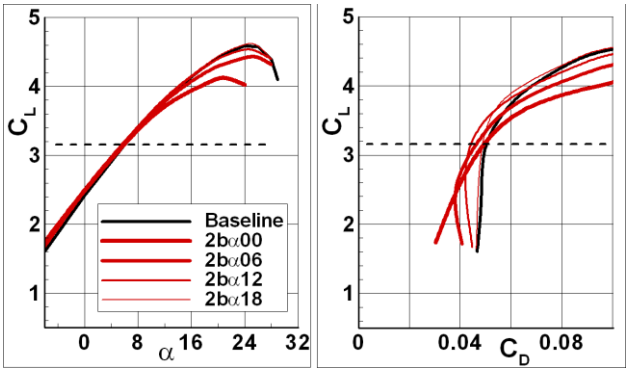

Fig. 12b. Aerodynamic Force of Slat Cove Fillers (Step 1)

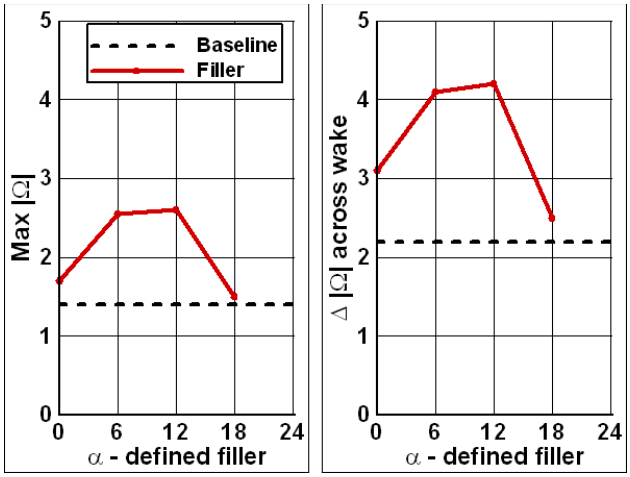

Fig. 13. Slat Wake Intensity of Cove Fillers (Step 1)

downstream of the upper trailing edge. According to Figure 12b, fillers 2bα06 and 2bα12 produce maximum lift coefficients within 0.2 from the baseline target. With respect to acoustics these two fillers prevent flow separation and the attendant wake shedding off lower side. However, stronger wakes now originate on the upper trailing edges of these slats (cut a). Referring to the flow fields in Figure 12a it appears that the flow in the gap region is slowed down considerably in the aft filler region. This occurs because of the relatively rapid geometrical change where the filler blends back to the original cove surface (defined by the shape of the separation bubble in the reattachment region in the respective baseline flow). Also, the cross sectional area of the channel between the slat and main element does not decrease monotonically, resulting in a region of flow deceleration. These two geometrical attributes result in inefficient flow along the gap. It is therefore conceivable that geometrical refinement of the fillers might be beneficial for enhanced maximum lift and reduced noise.

Step 2

Geometrical modifications in the aft portion of the fillers were made in step 2 for the 2bα00, 2bα06 and the 2bα12 configurations by inspection of the respective flow fields from Figure 12a. The results for 2bα06 is shown in Figure 14 in which the modified fillers are

denoted by the suffix "-cove". The vorticity contours obtained for α=6º indicate that the flow in the gap region has dramatically improved, with a thinner viscous layer on the lower surfaces of the slats. The flow coming out of the gap towards the upper side of the main element is more uniform and contains higher momentum, leading to a more efficient interaction with the viscous layers of main element and the flap. Marked gains in $C_{L\ Max}$ are realized for all three fillers, with the largest increment obtained for the 2bα00 filler ($\Delta C_{L\ Max}$ ~0.4). As expected, the slat is a major

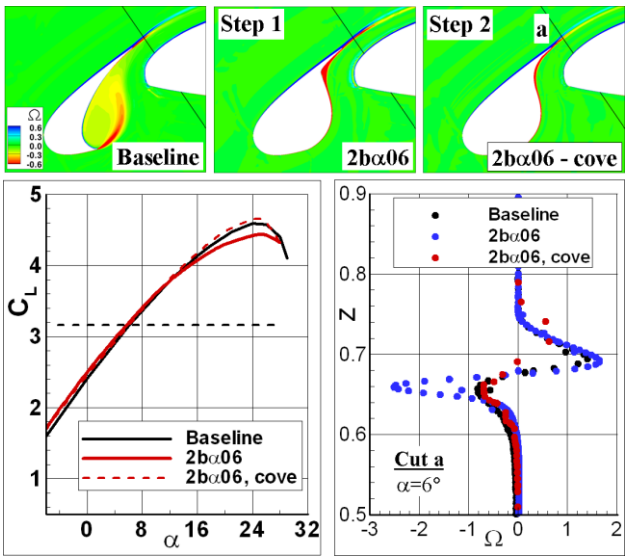

Fig. 14. Refined Slat Filler 2ba06 (Step 2)

determinant of maximum lift and therefore the refined fillers are very effective in producing $C_{L\ Max}$ comparable to the baseline.

The refined slats produce more symmetrical wakes (peak-to-peak vorticity magnitudes across the wake) relative to the original fillers. Moreover, wake intensities are significantly reduced, even relative to the baseline airfoil. It is quite possible that the refined fillers will consequently generate even lesser noise. Figure 15 presents the parametric summary of the cove fillers illustrating the improvements realized in Step 2.

The lift and drag characteristics of the refined slat fillers which meet the $C_{L\ Max}$ criteria

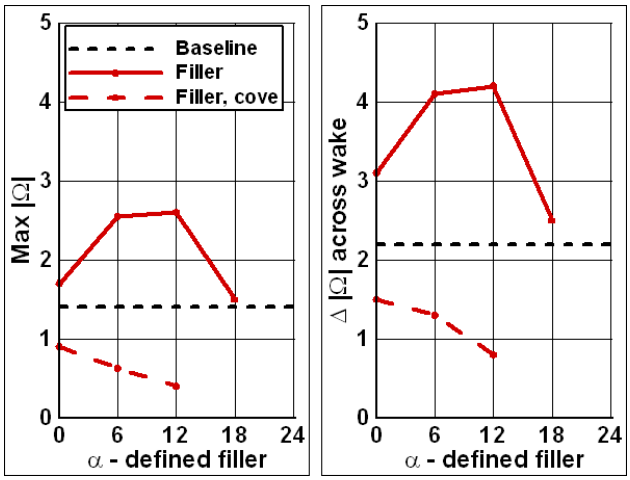

Fig. 15. Slat Wake Intensity of Cove Fillers

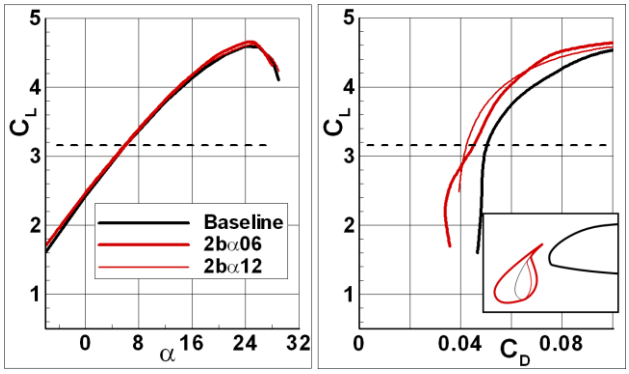

Fig. 16. Aerodynamic Forces of Candidate α-Fillers

are shown in Figure 16 (note that the suffix "-cove" is dropped, and 2bα06 and 2bα12 refer now to the refined slats).

5.2.3.b Other Optional Fillers

The size of the filler is highly dependent on the choice of α. Smaller fillers are obtained from high α cases since the size of the separation bubble is inversely proportional to global circulation. It can be inferred from Figure 17 that filler size is a very important parameter in regard to mechanization of the slat system. Obviously, smaller fillers will require less structural slat morphing.

In order to reduce the size of the cove filler it is instructive to explore other filler variants. The underlying factor affecting wake formation and wake intensity is the cusp trailing edge on the lower side of the slat. Removing the trailing edge and replacing it with smooth filler that gradually blends to the cove surface might

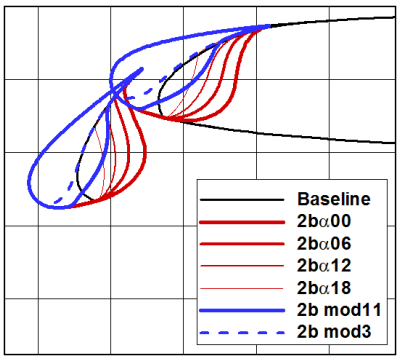

Fig. 17. Various Fillers in Stowed and Deployed Positions

be beneficial. This geometry is denoted 2b-mod11 in Figure 17. Another variation with a slat that is smaller than the original one and does not require structural morphing is denoted 2b-mod3. Obviously, both of these fillers will require a small deployable element on the lower surface so that the cruise mold line is preserved when the slat is retracted.

Figures 18a-b show the flow fields and wake profiles for the two slat options. Similar to the α-filler cases, the two-steps approach was used to obtain a refined geometrical definition for 2b-mod11. The simulations indicate that the flow does not separate on either one of the slats over the entire range of angles-of-attack. Maximum lift of both slats is very similar to the baseline airfoil. Also, the refined definition of 2b-mod11 helps reduce slat wake intensity. In

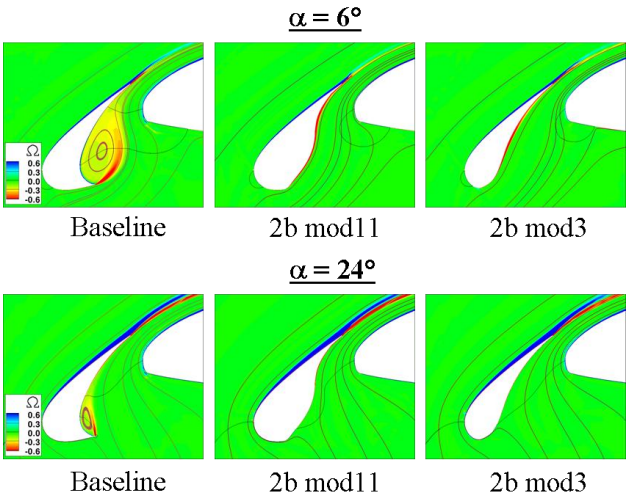

Fig. 18a. Flow Fields of 2b-mod11 and 2b-mod3 Fillers at the Nominal Condition and Near $C_{L\ Max}$

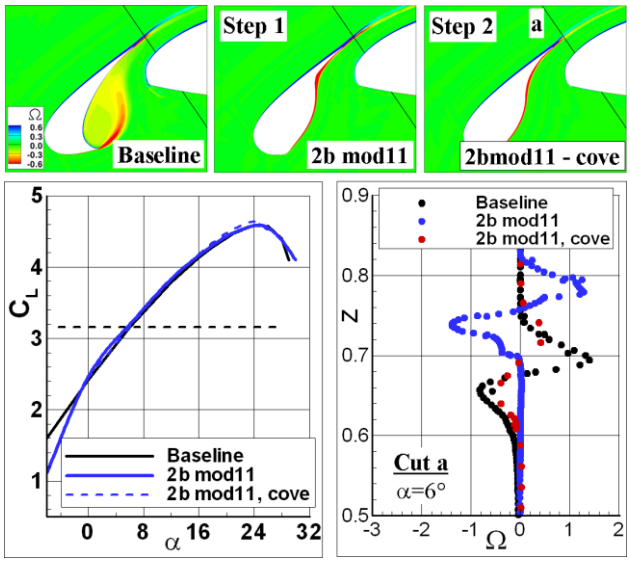

Fig. 18b. Refined Slat Filler 2b mod11

the 2b-mod3 case, however, it is not at all clear that this will necessarily lead to reduced noise since the gap between the slat and main wing element is now larger.

5.3 Candidate Wing LE Configurations

The current study helped identify concepts of low noise LE devices from the aerodynamics point of view. A comparative summary of sectional aerodynamic forces of promising slat candidates is presented in Figure 19. It includes an extended drooped LE which requires AFC for good stall characteristics. Several slat cove filler shapes have been systematically developed such that their lift characteristics at the nominal landing condition and at stall are equivalent to that of the baseline section.

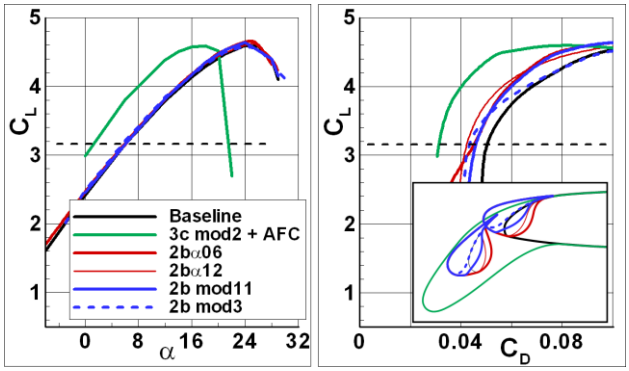

Fig. 19. Aerodynamic Forces of Candidate LE Devices for Low Noise

6 Conclusions

The aerodynamic characteristics of candidate high-lift concepts were assessed for wing sectional geometries. Geometrical modifications for enhanced performance were confined to slat modifications. Cruise mold lines have not been altered. This study focused on identifying gross effects and therefore the aerodynamic performance of potential concepts should be considered conservative. It is conceivable that further improvement can be realized by subsequent optimization through flap deflection, geometrical refinements and control of gap and overhang for both slat and flap elements. In the case of the extended droop slat, an optimized AFC implementation will be vital in order to evaluate actuation modes and to guide the placement of the individual ports for maximum cumulative effect within realistic power budget limits.

Knowledge based engineering was employed throughout the aerodynamic design to qualitatively estimate noise benefits of the proposed configurations. A thorough subsequent study is required to accurately establish potential acoustics gains. Clearly, the prospects of implementation of practical low noise LE devices will depend on technological advances in the areas of improved mechanical systems or morphing structures.

7 Acknowledgement

This study was funded by NASA Multi-Objective Leading Edge Concepts program where Dr. Travis Turner was the contract monitor.

8 References

[1] Andreou C, Graham W and Shin H. Aeroacoustic comparison of airfoil leading edge high-lift geometries and supports. AIAA Paper 2007-230.

[2] Buning P G , Chiu I T , Obayash S, Rizk Y M and Steger J L. Numerical simulation of the integrated space shuttle vehicle in ascent. AIAA Paper 1988-4359.

[3] Shmilovich A and Yadlin Y. Flow control for the systematic buildup of high lift systems. *Journal of Aircraft*, vol. 45 no.5 (1680-1688), 2008.

[4] Khodadoust A and Shmilovich A. High Reynolds numbers simulations of distributed Active Flow Control for a high-lift system. AIAA Paper 2007-4423.

[5] Lin C J and Dominik J C. Parametric investigation of a high-lift airfoil at high Reynolds numbers. *Journal of Aircraft*, vol. 34 no.4 (485-491), 1997.

[6] Krzysiak A. Control of flow separation using self-supplying air-jet vortex generators. *AIAA Journal*, vol. 46 no.9 (2229-2234), 2008.

[7] Prince S A, Khodagolian V, Singh C, Moir S and Kokkalis A. Aerodynamic stall suppression on aerofoil sections using passive air jet vortex generators. *26th International Congress of the Aeronautical Sciences*, Paper #030, 2008.

[8] Khodadoust A and Washburn A. Active control of flow separation on a high-lift system with slotted flap at high Reynolds number. AIAA Paper 2007-4424.

[9] Shmilovich A and Yadlin Y. Active Flow Control for practical high-lift systems. AIAA Paper 2007-3971.

[10] Streett C L, Casper J H, Lockard D P, Khorrami M R, Stoker R W, Elkoby R, Wenneman W F and Underbrink J R. Aerodynamic noise reduction for high-lift devices on a swept wing model. AIAA Paper 2006-212.

[11] Kolb A, Faulhaber P, Drobietz R and Grunewald M. Aeroacoustic Wind tunnel measurements on a 2D high-lift configuration. AIAA Paper 2007-3447.

[12] Imamura1T, Ura H, Yokokawa Y, Enomoto S, Yamamoto K and Hirai T. Designing of slat cove filler as a noise reduction device for leading-edge slat. AIAA Paper 2007-3473.

9 Copyright Statement